Special issue article

SURFACE and INTERFACE ANALYSIS

Received: 21 February 2017 Revised: 6 April 2017 Accepted: 8 April 2017 Published online in Wiley Online Library: 12 May 2017

(wileyonlinelibrary.com) DOI 10.1002/sia.6239

Advanced analysis of copper X-ray photoelectron spectra

Mark C. Biesinger*

Chemical state X-ray photoelectron spectroscopic analysis of copper species is challenging because of the complexity of the 2p spectra resulting from shake-up structures for Cu(II) species and overlapping binding energies for Cu metal and Cu(I) species. This paper builds upon and extends previously published X-ray photoelectron spectroscopy curve-fitting and data analysis procedures for a wide range of copper containing species. Steps undertaken include the following: (i) an examination of existing Cu $2p_{3/2}$ main peak and Cu $2p_{3/2}$ – Cu $L_3M_{4,5}M_{4,5}$ Auger parameter literature data, (ii) analysis of a series of quality standard samples, (iii) curve-fitting procedures for both the Cu $2p_{3/2}$ and the Cu $L_3M_{4,5}M_{4,5}$ spectra (as well as associated anions), (iv) calculations that determine the amount of Cu(II) species in a mixed oxidation state system, (v) calculations and necessary data for thin film mixed oxide/hydroxide thickness measurements, and (vi) a presentation of literature and standard sample values in a Wagner (chemical state) plot. Copyright © 2017 John Wiley & Sons, Ltd.

Keywords: copper; XPS; X-ray photoelectron spectroscopy; peak-fitting; oxides; Auger; Wagner plot

Introduction

From antiquity to modern day, copper and its alloys have been integral to civilization. Easily molded and shaped, an efficient conductor of electricity and heat, and resistant to corrosion, copper has a multitude of uses in domestic, industrial, and high tech applications.[1] In 2015, world mine production was 18.7 million metric tons.[2]

Copper clad steel containers are being considered as a means to store high-level nuclear waste in a long-term deep geologic repository. Assessment of the integrity and longevity of these containers in a multi-barrier system involves a combination of experimental and modelling approaches. These include the application of a wide range of electrochemical techniques often under hostile conditions, such as high temperatures in the presence of aggressive environments. These methods are supplemented by various surface and near-surface analytical techniques, such as X-ray photoelectron spectroscopy (XPS), Auger spectroscopy, SEM, neutron reflectometry, and others. XPS, in particular, has been essential for the characterization of the chemistries involved with thin oxide film growth.[3] The need for improved XPS analysis of copper spectra has also been noted with procedures recently developed to curve-fit the full Cu 2p spectrum using standard spectra line-shapes for graphite-supported ultra-small copper nanoparticles.[4]

Chemical state determination using XPS has become routine for most of the elements in the periodic table. Binding energy (BE) databases, such as the National Institute of Standards and Technology (NIST) Database[5] or the Phi Handbook[6], generally provide sufficient data for the determination of chemical state for uncomplicated (i.e. single peak) spectra. However, the transition metal 2p spectra pose several problems that these databases do not adequately address, specifically, shake-up structure, multiplet splitting, and plasmon loss structure, all of which can complicate both interpretation and quantitation of the chemical states present. For example, fitting parameters such as peak widths and asymmetries, which are vital for curve-fitting of complex, mixed metal/oxide systems, are not included in these databases. To remedy this, practical methods that combine theoretical and experimental information to produce curve-fitting procedures have been developed and reported for species that show minimal or no multiplet splitting (Sc, Ti, V, Cu, and Zn)[7] and for those that show significant multiplet splitting (Cr[8,9], Mn,[8] Fe[8,10], Co,[8] and Ni[8,11,12]).

This paper builds upon and extends these types of procedures for a wide range of copper containing species. Steps undertaken include the following: (i) an examination of existing Cu $2p_{3/2}$ main peak and Cu $2p_{3/2}$ – Cu $L_3M_{4,5}M_{4,5}$ Auger parameter literature data, (ii) analysis of a series of quality standard samples, (iii) curve-fitting procedures for both the Cu $2p_{3/2}$ and the Cu $L_3M_{4,5}M_{4,5}$ spectra (as well as associated anions), (iv) calculations that determine the amount of Cu(II) species in a mixed oxidation state system, (v) calculations and necessary data for thin film mixed oxide/hydroxide thickness measurements, and (vi) a presentation of literature and standard sample values in a Wagner (chemical state) plot.

In quantification of thin films by XPS, compositional and chemical state variation with depth can introduce significant errors, recently reviewed by Powell and Jablonski[13], due, in part, to inelastic mean free path (IMFP) differences associated with the different chemistries. Methods to explore layered structures (e.g. QUASES)[14] and evaluate multiphase particles[15] have been used in some of our previous work.[11,16–19] In this paper, we have focused on improved chemical state recognition and quantitative estimation. The

* *Correspondence to: Mark C. Biesinger, Surface Science Western, The University of Western Ontario, 999 Collip Circle, Suite LL31, London N6G 0J3, Ontario, Canada. E-mail: biesingr@uwo.ca*

Surface Science Western, The University of Western Ontario, London N6G 0J3, ON, Canada

procedures can be used in subsequent depth analysis.[11,16] BE calibration procedures, essential to this process, particularly for sample charge referencing, are also described and discussed.

Experimental

The XPS analyses were carried out with both Kratos AXIS Ultra and Kratos AXIS Nova spectrometers (Kratos Analytical, Manchester, UK) using a monochromatic Al Kα source (15 mA, 14 kV). Instrument work functions were calibrated to give an Au $4f_{7/2}$ metallic gold BE of 83.95 eV. The spectrometer dispersion was adjusted to give a (BE) of 932.63 eV for metallic Cu $2p_{3/2}$. The Kratos charge neutralizer system was used for all analyses as needed. Charge neutralization was deemed to have been fully achieved by monitoring the C 1s signal for adventitious carbon. A sharp main peak with no lower BE structure is generally expected. Instrument base pressure was 8×10^{-10} Torr. High-resolution spectra were obtained using an analysis area of ≈300 × 700 μm and a 20-eV pass energy. This pass energy corresponds to a Ag $3d_{5/2}$ full width at half maximum (FWHM) of 0.55 eV.

A single peak [Gaussian (70%) – Lorentzian (30%)], ascribed to alkyl type carbon (C–C, C–H), was fitted to the main peak of the C 1s spectrum for adventitious carbon. A second peak is usually added that is constrained to be 1.5 eV above the main peak and of equal FWHM to the main peak. This higher BE peak is ascribed to alcohol (C–OH) and/or ester (C–O–C) functionality. Further, high BE components (e.g. C=O, 2.8–3.0 eV above the main peak, C–O–C, 3.6–4.3 eV above the main peak) can also be added if required. Spectra from insulating samples have been charge corrected to give the adventitious C 1s spectral component (C–C, C–H) a BE of 284.8 eV. The process has an associated error of ±0.1–0.2 eV.[20] Experience with numerous conducting samples and a routinely calibrated instrument has shown that the non-charge corrected C 1s signal generally ranges from 284.7 eV to as high as 285.2 eV. The spectra for argon ion sputter cleaned metallic species are referenced to Au $4f_{7/2}$ at 83.95 eV. The powder (or consolidated) samples were not sputter cleaned prior to analysis, as it is well known that this can cause reduction of oxidized species.

Spectra were analyzed using CasaXPS software[21] (version 2.3.14). Gaussian (Y %) – Lorentzian (X %), defined in CasaXPS as GL(X), profiles were used for each component. The best mixture of Gaussian–Lorentzian components will vary depending on the instrument and resolution (pass energy) settings used as well as on the natural line-width of the specific core hole. Changes to the Gaussian–Lorentzian mix do not, in general, constitute large peak area changes. If the mix is in a reasonable range and applied consistently, reasonable results are obtained. A standard Shirley background is used for all reference sample spectra.

Powder and metal samples of the highest purity readily available were purchased from Alfa Aesar (Haverhill, Massachusetts, USA). Where available, samples that were received ampouled or packed under argon were introduced into the XPS instrument via an attached argon filled glove box (CuI, CuCl, $CuCl_2$, and CuF_2). CuCl, which is light sensitive, was introduced and analyzed in a darkened room/chamber. The chalcocite (Gardner Mine, Bisbee, Arizona) specimen was obtained from Mineralogical Research Company (San Jose, California, USA) and was ground in a mortar under Ar prior to analysis. All powder samples were mounted on non-conductive adhesive tape. All Cu(II) species were pre-cooled to and held at −140 to −150 °C for analysis as previous work[7] has shown that sample cooling sustainably slows X-ray degradation of Cu(II) to Cu(I). Other strategies were also employed to limit X-ray exposure for these samples (e.g. high-resolution spectra taken before survey scans, minimal scans taken for sufficient signal to noise). The metal sample was sputter cleaned using a 4 kV argon ion beam to remove all oxide and carbonaceous species. Cu_2O, $Cu(OH)_2$, and CuO samples were checked for purity by powder X-ray diffraction using an Inel diffractometer (Artenay, France) equipped with a XRG 3000 generator and CPS 120 curved position sensitive detector using monochromated Cu Kα radiation (λ = 1.54056 Å). The remaining samples were checked for purity by using XPS survey scan (elemental) data, presented in Appendix I.

Powder and polycrystalline materials were used to remove the possibility of photoelectron diffraction effects, which can influence splitting patterns.[22,23] They are also more representative of most of the samples in practical analyses of air-exposed multi-component materials.

Results and discussion

Literature values

Table 1 lists Cu $2p_{3/2}$ BE and modified Auger parameter values from a survey of literature sources compiled in the NIST Database.[5] Of note here is the statistically similar BE values for the Cu metal and the majority of Cu(I) species. The use of the modified Auger parameter ($2p_{3/2}$, $L_3M_{45}M_{45}$) and an inspection of the Auger peak-shape do allow for a more accurate assignment for these species

Table 1. Cu $2p_{3/2}$ and Cu $2p_{3/2}$ – Cu $L_3M_{4,5}M_{4,5}$ Auger parameter literature values from Cu species (compiled from Ref. [5])

Compound	Cu $2p_{3/2}$ (eV) (lit. ave)	Std. dev. (+/− eV)	# of citations	Modified Auger parameter (lit. ave.)	Std. dev. (+/− eV)	# of citations
Cu(0)[a]	932.6	0.2	27	1851.2	0.2	23
Cu_2O	932.4	0.2	18	1849.2	0.3	10
CuO	933.6	0.4	18	1851.5	0.4	10
$Cu(OH)_2$	934.8	0.5	2	1851.3	—	1
CuF_2	936.4	0.4	12	1851.7	0.3	10
CuCl	932.4	0.2	6	1847.8	0.2	4
$CuCl_2$	934.8	0.7	8	1850.2	0.2	4
CuBr	932.3	0.2	2	—	—	—
$CuBr_2$	934.3	0.7	8	1850.8	0.6	6
CuI	932.2	0.4	2	—	—	—
$CuCO_3$	935.0	—	1	1851.3	—	1
CuCN	933.0	0.2	2	1847.6	0.1	2
Cu_2Se	932.1	0.3	3	1849.9	0.6	2
$CuInSe_2$	932.2	0.4	4	—	—	—
$CuInS_2$	932.6	0.4	3	1849.5	0.2	5
CuSe	932.0	—	2	1850.4	—	1
$Cu(NO_3)_2$	935.5	—	2	1850.8	—	1
$CuSO_4$	935.3	0.5	4	1851.4	0.2	4
CuS	932.2	0.2	8	1850.3	0.2	3
Cu_2S	932.5	0.3	10	1849.8	0.2	3
$CuFeS_2$	932.2	0.2	3	1850.1	—	1
Cu_3AsS_3	932.3	—	2	—	—	—
YBa_2Cu_3O	934.7	1.2	5	—	—	—

[a]The ISO calibration standard is to set Cu $2p_{3/2}$ for the metal to 932.63 eV.

Table 2. Cu $2p_{3/2}$ (main peak only) and Cu $2p_{3/2}$ – Cu $L_3M_{4,5}M_{4,5}$ Auger parameter values from standard samples (20 eV pass energy)

Compound	Cu $2p_{3/2}$ (eV)	Std. dev. (+/− eV)	Modified Auger parameter (eV)	Std. dev. (+/− eV)
Cu(0)	932.63[a]	0.025[b]	1851.24	0.025[b]
Cu_2O	932.18	0.12	1849.17	0.03
CuO	933.76	0.11	1851.33	0.05
$Cu(OH)_2$	934.67	0.02	1850.92	0.09
CuF_2	936.38	0.15	1851.74	0.15
CuCl	932.34	0.03	1847.51	0.07
$CuCl_2$	935.30	0.11	1850.37	0.17
CuBr	932.27	0.14	1848.00	0.02
$CuBr_2$	934.50	0.14	1850.60	0.11
CuI	932.50	0.03	1848.84	0.01
$Cu_3(PO_4)_2$	935.85	0.07	1851.61	0.05
$Cu(NO_3)_{2.3}H_2O$	935.51	0.02	1850.49	0.15
$CuSO_4$	936.00	0.10	1851.91	0.10
Chalcocite (Cu_2S)	932.62	0.05	1849.84	0.03
Chalcopyrite ($CuFeS_2$)	932.14	0.02	1850.18	0.03

[a]ISO calibration standard 932.63 eV.

[b]As defined by Kratos calibration procedure. Note that this value is specified for the Kratos instruments used in this work. Other instruments may not have this accuracy. This will also not apply for Cu(0) in a non-conductive environment where calibration to other peaks are needed (e.g. adventitious carbon C 1s, which has an error of 0.1 to 0.2 eV associated with it).

Table 3. Copper compound standard samples anion binding energy, FWHM, and line-shape values

Compound	Element/ transition	Binding energy	Std. dev. (+/− eV)	FWHM (eV)	GL(x) for single peaks
Cu_2O	O 1s (Lat.)	530.20	0.01	1.23	30
	O 1s (Def.)	531.57	0.06	1.28	30
CuO	O 1s (Lat.)	529.68	0.05	0.89	30
	O 1s (Def.)	530.99	0.07	1.97	30
$Cu(OH)_2$	O 1s	531.24	0.06	1.59	30
CuF_2	F 1s	684.78	0.17	2.01	23
CuCl	Cl $2p_{3/2}$	199.15	0.05	0.95	27
$CuCl_2$	Cl $2p_{3/2}$	199.29	0.13	0.95	47
CuBr	Br $3d_{5/2}$	69.16	0.10	0.85	40
$CuBr_2$	Br $3d_{5/2}$	69.27	0.11	0.84	48
CuI	I $3d_{5/2}$	619.72	0.02	1.00	79
$Cu_3(PO_4)_2$	P $2p_{3/2}$	133.91	0.15	2.01	15
	O 1s	531.82	0.19	1.85	5
$Cu(NO_3)_{2.3}H_2O$	N 1s	407.52	0.06	1.34	59
	O 1s	533.36	0.08	1.69	50
$CuSO_4$	S $2p_{3/2}$	169.14	0.10	1.33	29
	O 1s	532.21	0.07	1.54	12
Chalcocite (Cu_2S)	S $2p_{3/2}$	161.84	0.05	0.80	25
Chalcopyrite ($CuFeS_2$)	S $2p_{3/2}$	161.28	0.02	0.60	60
	Fe $2p_{3/2}$	shows unique structure			

Lat., Lattice Oxide; Def., Defective Oxide; FWHM, full width at half maximum.

For Cu_2O and CuO defective oxide is ~32–36% of total oxygen.

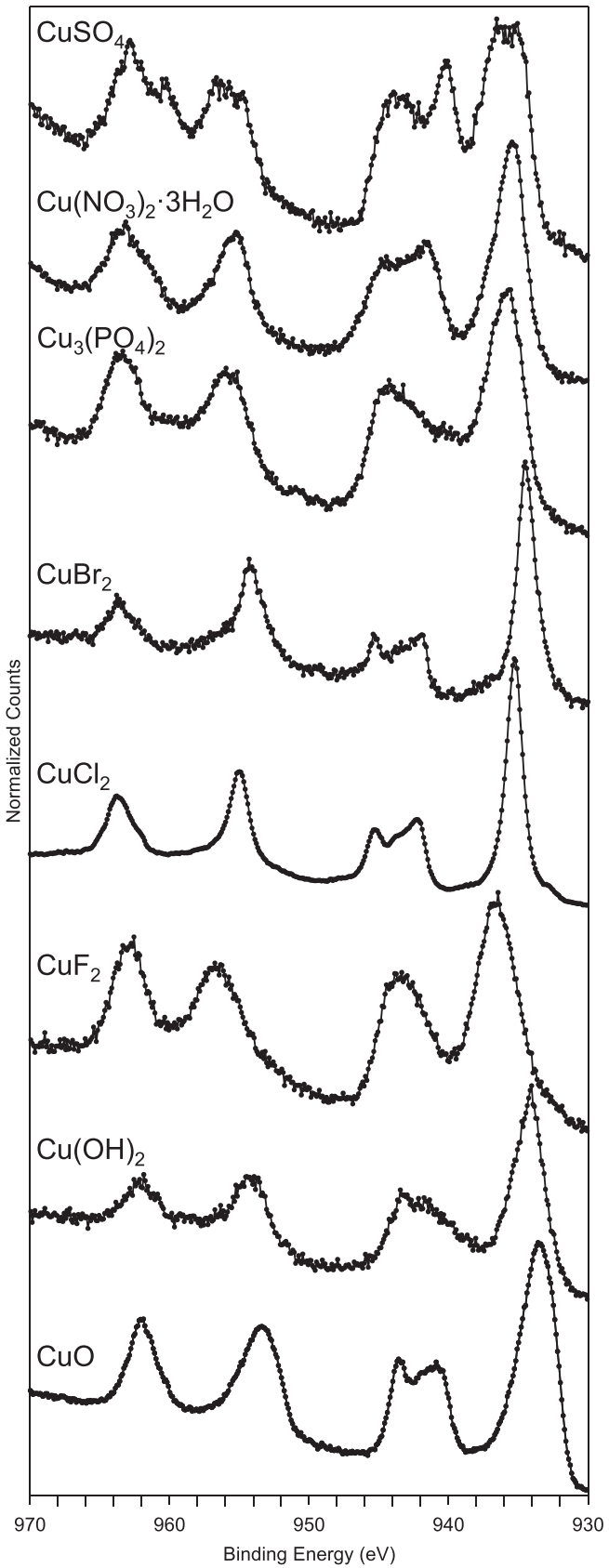

Figure 1. Cu $2p_{3/2}$ spectra for Cu(II) species.

and has been used effectively. Goh *et al.*[24] have shown (in their fig. 8) the distinctly different peak shapes of the X-ray generated Auger LMM spectra for copper as the metal, Cu_2S, and CuS. They also note the distinctive Cu $L_3M_{4,5}M_{4,5}$ peak at 916.5 eV for Cu_2O. Poulston *et al.*[25], in their study of surface oxidation and reduction of Cu_2O and CuO, have used both the Cu LMM and the Auger parameter to distinguish Cu(0), Cu(I), and Cu(II).

It should be noted that it has been shown that BE and Auger parameters for Cu (as well as Zn and Ti) can change for very thin films on certain substrates (interface effects) and for very small particles (particle size effects).[26,27] This will be an important point to consider for those studying catalysis and nano-compounds.

Standard sample analyses

Table 2 shows similar results to those shown in Table 1 from this work for a series of standard samples. A comparison of these standard sample values to literature values also serves as a secondary check of the standard sample's composition and lack of surface chemistry changes.

Table 3 presents anion species BE, FWHM, and peak-shape information for these samples. Figure 1 presents Cu $2p_{3/2}$ spectra for all studied Cu(II) compounds. As the Cu $2p_{3/2}$ and Cu $2p_{1/2}$ peaks are well separated, it is optimal to analyze and focus on only the Cu $2p_{3/2}$ portion of the Cu 2p spectrum. Figure 2 presents Cu $L_3M_{45}M_{45}$ Auger spectra for all studied compounds.

In this analysis (Table 2), a statistical separation of the Cu $2p_{3/2}$ peak position for Cu(0) and Cu_2O and other Cu(I) species is achieved. This should be expected, as most spectrometer calibration procedures include referencing to the ISO standard Cu metal line at 932.63 eV with deviation of this line set at ±0.025 eV. Curve-fitting of the Cu $2p_{3/2}$ line for both Cu metal and Cu_2O employed Gaussian (10%) – Lorentzian (90%) and Gaussian (20%) – Lorentzian (80%) peak-shapes, respectively, [defined in CasaXPS

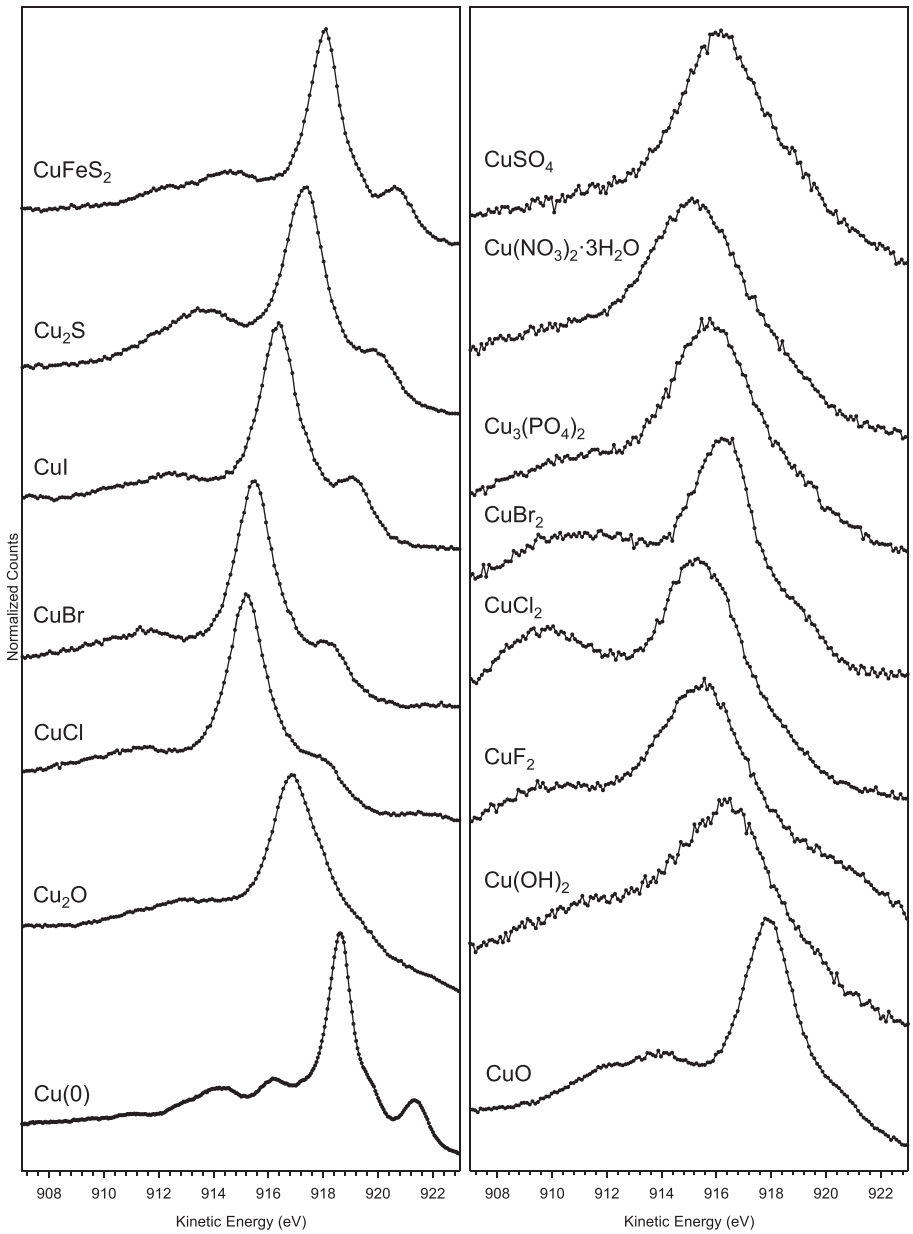

Figure 2. Cu $L_3M_{4,5}M_{4,5}$ spectra for (left) Cu(0), Cu(I) species, mineral samples, and (right) Cu(II) species.

Table 4. Cu $2p_{3/2}$ curve-fitting parameters

Compound	Peak 1 (eV)	%	FWHM (eV)	GL(x) value	Peak 2 (eV)	%	Δ Peak 2 − peak 1 (eV)	FWHM (eV)	Peak 3 (eV)	%	Δ Peak 3 − peak 2 (eV)	FWHM (eV)	Peak 4 (eV)	%	Δ Peak 4 − peak 3 2(eV)	FWHM (eV)	Peak 5 (eV)	%	Δ Peak 5 − peak 4 (eV)	FWHM (eV)
Cu(0)	932.63	100	0.83	90	—	—	—	—	—	—	—	—	—	—	—	—	—	—	—	—
Cu_2O	932.18	100	1.00	80	—	—	—	—	—	—	—	—	—	—	—	—	—	—	—	—
CuO	933.11	31	2.07	30	934.48	33	1.37	3.05	940.52	3	6.04	1.03	941.66	28	1.13	3.55	943.71	6	2.05	1.17
$Cu(OH)_2$	934.67	60	2.85	30	939.30	6	4.63	2.80	942.20	28	2.90	3.66	944.12	7	1.92	1.76	—	—	—	—
CuF_2	936.52	61	3.69	30	942.41	27	5.89	3.39	944.25	12	1.84	2.14	—	—	—	—	—	—	—	—
CuCl	932.34	100	1.07	78	—	—	—	—	—	—	—	—	—	—	—	—	—	—	—	—
$CuCl_2$	935.26	63	1.54	90	942.14	10	6.88	1.09	943.35	14	1.21	1.75	945.22	13	1.87	1.57	—	—	—	—
CuBr	932.27	100	1.00	80	—	—	—	—	—	—	—	—	—	—	—	—	—	—	—	—
$CuBr_2$	934.39	71	1.62	90	941.95	9	7.56	1.01	943.27	13	1.32	1.93	945.19	8	1.92	1.19	—	—	—	—
CuI	932.50	100	1.10	82	—	—	—	—	—	—	—	—	—	—	—	—	—	—	—	—
$Cu_3(PO_4)_2$	935.79	43	2.83	30	939.54	27	3.75	5.40	943.39	22	3.85	3.59	944.87	8	1.48	1.94	—	—	—	—
$Cu(NO_3)_{2.3}H_2O$	935.39	43	2.27	30	937.40	11	2.01	2.22	941.53	24	4.13	2.70	944.52	23	2.99	3.14	—	—	—	—
$CuSO_4$	934.66	7	1.35	30	936.33	46	1.67	3.54	940.18	16	3.85	1.80	942.72	22	2.54	3.07	944.63	9	1.91	1.93
Chalcocite (Cu_2S)	932.62	100	1.16	72	—	—	—	—	—	—	—	—	—	—	—	—	—	—	—	—
Chalcopyrite ($CuFeS_2$)	932.14	100	0.95	76	—	—	—	—	—	—	—	—	—	—	—	—	—	—	—	—

FWHM, full width at half maximum.

as GL(90) and GL(80)]. Peak-shapes for all Cu(I) species are reported in Table 4.

Curve-fitting the Cu $2p_{3/2}$ spectrum

Many authors use the presence of the well-known shake-up satellite found in Cu 2p spectra as an indication of the presence of Cu(II) species.[28–35] Some choose to use this information in only a qualitative fashion.[28],[29],[30],[31] Others taking a quantitative approach have peak fit the main $2p_{3/2}$ peak with two to three separate components, the metal, Cu(I), and Cu(II) but ignore the contribution of the shake-up satellite.[32],[33] Kundakovic and Flytzani-Stephanopoulos[34] use the presence of the shake-up peak to estimate the amount of CuO but do not elaborate on the method by which the amounts given are obtained. Salvador *et al.*[35] use ratios of the main $2p_{3/2}$ peak to the shake-up peak to qualitatively compare the amount of oxidation of copper in $YBa_2Cu_3O_{7-x}$ samples to a fully oxidized CuO standard sample.

It is possible to fit the $2p_{3/2}$ spectrum using a set of constrained peaks that simulate the entire peak-shape (including the shake-up components) for the Cu(II) species present (Table 4), similar to the procedures for Cr,[8,9] Mn,[8] Fe,[8,10] Co,[8] and Ni.[8,10,12] Full spectral fitting parameters for all species are presented in Table 4. In practice, quantifying a mix of Cu(0), Cu(I), and Cu(II) species would require precise constraints on BE, FWHM, and peak-shape parameters. Speciation will be possible for relatively simple combination of species. Resolution of these components will be difficult with larger amounts of Cu(II) compounds present because of the overlap of peaks for these three components. Speciation of the Cu(I) species present, if a variety of anions are possible (e.g. O and Cl or Br is present in the survey spectrum), will also be problematic as there is a statistical overlap of the Cu $2p_{3/2}$ BE of most Cu(I) species. However, if Cu(I) species dominate the Cu $2p_{3/2}$ spectrum (i.e. only low amounts of Cu(II) species are present as indicated by the shake-up structure), then the use of the Auger parameter is possible for species confirmation.

[Cu(0) + Cu(I)]: Cu(II) calculations

A study of the surface chemistry of the flotation separation of chalcocite (Cu_2S) from heazelwoodite (Ni_3S_2) employed a fitting procedure and calculation that quantifies the amount of Cu(II) species present on the surface of Cu(I) sulfide[36] as first developed and now described by Jasieniak and Gerson.[37] The calculation takes into account the photoelectron yields from both the main $2p_{3/2}$ peak and the shake-up peak and is based on main peak/shake-up peak ratios derived from $Cu(OH)_2$ standard spectra. X-ray reduction of the Cu(II) samples has also been considered in this work.

Quantification of the amount of Cu(II) species on a Cu(0) or Cu(I) containing surface does appear to be possible. If, for example, a Cu metal surface is oxidized to Cu(II), the shake-up structure associated with the Cu(II) species can be used for a Cu(0):Cu(II) quantification. Alternatively if Cu(II) species and Cu(I) species are present, the Cu(I):Cu(II) ratio can be determined. This method[36] of Cu(0):Cu(II) {or Cu(I):Cu(II), or in general [Cu(0) + Cu(I)]:Cu(II)} determination depends on shake-up peaks that are present in the spectra of d^9 Cu(II) containing samples but are absent in d^{10} Cu(0) or Cu(I) spectra. Shake-up peaks may occur when the outgoing photoelectron simultaneously interacts with a valence electron and excites it to a higher-energy level. The kinetic energy of the core electron is then slightly reduced giving a satellite structure a few eV below (higher on the calculated BE scale) the core level

position.[38] Hence, these electrons are part of the total Cu 2p emission and should be included in both total Cu and relative chemical state speciation.

The main emission line (A) (see for example Fig. 3) contains both Cu(0) and Cu(I) and Cu(II) contributions but the shake-up satellite intensity (B) is entirely from Cu(II). The total intensity from Cu(II) species is represented in the combination of the signals from the direct photoemission (A1) and the shaken-up photoemission (B).

Accurate [Cu(0) + Cu(I)]:Cu(II) ratios for samples containing a mixture of species rely on determining an accurate ratio of the main peak/shake-up peak areas ($A1_s/B_s$) for a 100% pure Cu(II) sample. With a reliable value of $A1_s/B_s$ obtained for $Cu(OH)_2$ or CuO (or other Cu(II) species where all copper present is in the Cu(II) state), the relative concentrations of [Cu(0) + Cu(I)] and Cu(II) species present on a surface that contains both species can be obtained by the following simple equations:

$$\begin{aligned}\%(\mathrm{Cu}(0)+\mathrm{Cu}(\mathrm{I})) &= A2/(A+B)^{*}100 \\ &= (A-A1)/(A+B)^{*}100 \\ &= (A-(A1_s/B_s)B)/(A+B)^{*}100 \end{aligned} \quad (1)$$

$$\begin{aligned}\%\mathrm{Cu}(II) &= (B+A1)/(A+B)^{*}100 \\ &= B(1+(A1_s/B_s))/(A+B)^{*}100 \end{aligned} \quad (2)$$

where B is the area of the shake-up peak and A is the total area of the main peak.

Collected $A1_s/B_s$, values at 20 eV pass energy are as follows: $Cu(OH)_2$ 1.57, CuO 1.89, CuF_2 1.56, $CuCl_2$ 1.63, and $CuBr_2$ 2.45. Determination of which $A1_s/B_s$ value to use must be made by an assessment of all available data including shake-up peak-shape, survey data, and anion spectral data (i.e. an assessment of which Cu(II) species is present must be made). For examples,

i if $Cu(OH)_2$ or CuO is suspected two ways of confirming this are as follows:
   A The peak-shape and main peak to shake-up peak separation is quite different for $Cu(OH)_2$ and CuO.
   B A confirmatory check of the O 1s spectrum must also show the presence or absence of the hydroxide or lattice oxide peak.

ii If a species such as $CuCl_2$ is suspected, chloride must be present in the survey scan in sufficient amounts and bromine should be absent as $CuCl_2$ and $CuBr_2$ have similar looking shake-up structures.

If the Cu(0) or Cu(I) signal is relatively strong, (and the sample is conducting) some assessment of which is present in the sample may be made based on the BE of the $2p_{3/2}$ peak. For a well-calibrated spectrometer, the BE for Cu(0) should be almost exact. Any deviation from this should then be due to the presence of Cu(I). Spectrometer calibration using sputter cleaned Cu metal would be appropriate when these types of analyses are carried out. If levels of Cu(II) are relatively low, it is possible to confirm the assignment of Cu(0) or Cu(I) using the Auger parameter (Tables 1 and 2). This is also required for a non-conductive surface where charge correction to adventitious carbon will make assignment more challenging. An examination of the Auger peak-shape can also give clues to the nature of Cu(0) or Cu(I) species present.

An example of the results of this type of analysis is presented in Fig. 3. In the Cu $2p_{3/2}$ spectrum, the areas of peaks A (94%) and B (6%) are calculated using Shirley backgrounds placed across the main (A) and shake-up (B) peaks with the calculations giving 85% Cu(0) + Cu(I) and 15% Cu(II) using an $A1_s/B_s$, values of 1.57 for $Cu(OH)_2$. Error in this method depends greatly on the signal to noise of the spectrum and positioning of the backgrounds. Error will increase as the shake-up peak size decreases and an error of at least +/−5% is likely for this sample result. Visual examination of the overall Cu $L_3M_{4,5}M_{4,5}$ peak-shape and comparison to the reference spectra in Fig. 2 suggests that there is a mix of Cu(0) and Cu_2O (with a small amount of Cu(II) species proven to be present by the Cu $2p_{3/2}$ spectrum analysis).

Curve-fitting the Cu $L_3M_{4,5}M_{4,5}$ Auger spectrum

Earlier work[25,39,40] has shown that a clear differentiation of species can be made using the Cu $L_3M_{4,5}M_{4,5}$ Auger spectral line-shapes. Other works of Ni[41] and Ga[42] have also clearly shown that Auger spectral line-shapes and positions vary with species oxidation state and ligand variety. Thus, as is performed with the $2p_{3/2}$ line-shapes for varying species, it is possible to use curve-fitting procedures of

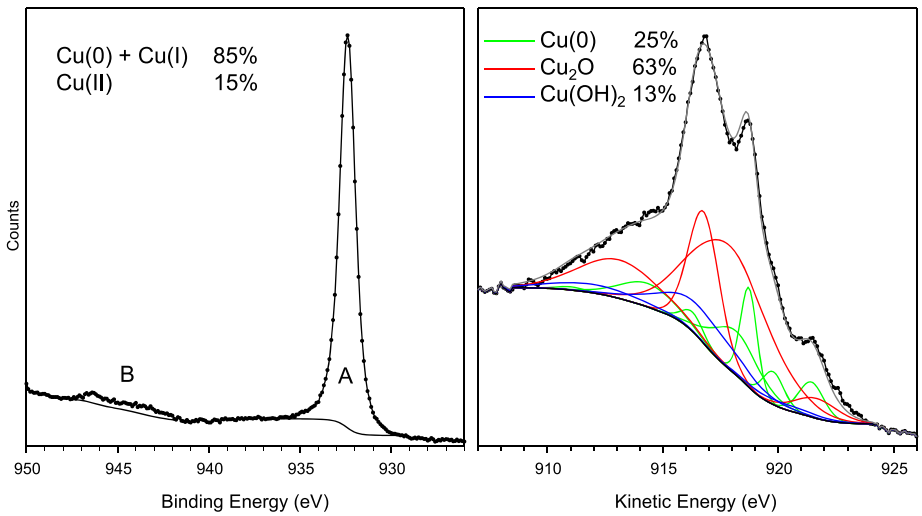

Figure 3. Cu $2p_{3/2}$ (left) and Cu $L_3M_{4,5}M_{4,5}$ (right) spectra from a sample of as received cold sprayed copper on a steel substrate. The Cu $2p_{3/2}$ main peak (A) and shake-up peak (B) areas were measured at 94% and 6% corresponding to calculated values of 85% [Cu(0) + Cu(I)] and 15% Cu(II) species. Curve-fitting of the Cu $L_3M_{4,5}M_{4,5}$ spectrum gave results of 25% Cu(0), 63% Cu_2O, and 13% $Cu(OH)_2$.

Table 5. Cu $L_3M_{4,5}M_{4,5}$ curve-fitting parameters (peak positions in kinetic energy)

Compound	Peak 1 (eV)	%	FWHM (eV)	GL(x) value	Peak 2 (eV)	%	Δ Peak 2 – peak 1 (eV)	FWHM (eV)	Peak 3 (eV)	%	Δ Peak 3 – peak 2 (eV)	FWHM (eV)	Peak 4 (eV)	%	Δ Peak 4 – peak 3 (eV)	FWHM (eV)	Peak 5 (eV)	%	Δ Peak 5 – peak 4 (eV)	FWHM (eV)	Peak 6 (eV)	%	Δ Peak 6 – peak 5 (eV)	FWHM (eV)	Peak 7 (eV)	%	Δ Peak 7 – peak 6 (eV)	FWHM (eV)
Cu(0)	921.35	13	1.28	30	919.70	10	−1.65	1.11	918.64	23	−1.06	0.84	918.09	29	−0.55	2.32	916.20	6	−1.89	1.10	914.26	18	−1.94	2.78	910.94	1	−3.32	1.42
Cu_2O	921.74	5	2.20	30	917.95	55	−3.79	4.01	916.86	23	−1.09	1.57	913.19	17	−3.67	4.10	—	—	—	—	—	—	—	—	—	—	—	—
CuO	919.92	26	3.68	30	917.86	40	−2.06	2.04	914.22	31	−3.64	4.66	911.37	3	−2.85	2.22	—	—	—	—	—	—	—	—	—	—	—	—
$Cu(OH)_2$	920.11	10	3.32	30	916.52	69	−3.59	4.06	911.93	21	−4.59	4.47	—	—	—	—	—	—	—	—	—	—	—	—	—	—	—	—
CuF_2	920.07	13	3.43	30	915.59	65	−4.48	4.12	910.26	22	−5.33	4.54	—	—	—	—	—	—	—	—	—	—	—	—	—	—	—	—
CuCl	917.96	15	1.85	30	916.35	15	−1.61	1.57	915.21	37	−1.14	1.32	914.15	8	−1.06	1.46	911.75	25	−2.40	4.95	—	—	—	—	—	—	—	—
$CuCl_2$	918.55	8	2.53	30	915.54	62	−3.01	3.37	911.17	19	−4.37	3.45	909.07	11	−2.10	2.61	—	—	—	—	—	—	—	—	—	—	—	—
CuBr	918.18	17	1.76	30	916.70	11	−1.48	1.20	915.56	37	−1.14	1.31	914.74	13	−0.82	1.71	911.79	23	−2.95	4.30	—	—	—	—	—	—	—	—
$CuBr_2$	919.04	10	1.95	30	916.36	52	−2.68	2.59	912.53	32	−3.83	4.82	909.62	7	−2.91	2.68	—	—	—	—	—	—	—	—	—	—	—	—
CuI	919.09	19	1.68	30	917.54	11	−1.55	1.21	916.44	29	−1.10	1.22	915.91	22	−0.53	1.92	912.73	19	−3.18	4.01	—	—	—	—	—	—	—	—
$Cu_3(PO_4)_2$	919.11	13	3.06	30	915.86	67	−3.25	3.59	911.17	21	−4.69	4.76	—	—	—	—	—	—	—	—	—	—	—	—	—	—	—	—
$Cu(NO_3)_{2,3}H_2O$	918.64	11	3.13	30	915.33	74	−3.31	4.04	910.52	14	−4.81	4.55	—	—	—	—	—	—	—	—	—	—	—	—	—	—	—	—
$CuSO_4$	918.59	28	4.08	30	916.05	43	−2.54	3.02	913.37	30	−2.68	7.19	—	—	—	—	—	—	—	—	—	—	—	—	—	—	—	—
Chalcocite (Cu_2S)	919.91	14	1.81	30	918.70	3	−1.21	1.01	917.37	42	−1.33	1.61	916.00	2	−1.37	1.07	913.88	38	−2.12	4.49	—	—	—	—	—	—	—	—
Chalcopyrite ($CuFeS_2$)	920.63	17	1.72	30	919.18	8	−1.45	0.96	918.15	26	−1.03	1.07	917.60	21	−0.55	1.78	914.77	24	−2.83	3.40	911.95	4	−2.82	1.87	—	—	—	—

FWHM, full width at half maximum.

the Cu $L_3M_{4,5}M_{4,5}$ Auger spectrum to elucidate and quantify the various Cu species present. Table 5 presents full Cu $L_3M_{4,5}M_{4,5}$ Auger spectral fitting parameters for all species analyzed. These fitting parameters can be used to reconstruct spectral peak-shapes in an appropriate fitting program by constraining the peak positions and/or peak separations, FWHM, and respective peak areas. FWHM are defined for each peak. Positions and areas are generally referenced to the first peak (e.g. peak 1 in Table 5) in the series for each species. This process is like using an actual line-shape from pure compounds but has more flexibility in its application. For instance, if charge referencing to C 1s is used, the first peak's position can be constrained to a window ~0.2 eV in width to account for the inaccuracy in this method. This will allow for the entire peak-shape to shift up or down as needed. If lower or higher resolution settings or a spectrometer with lower or higher resolution is used, the FWHMs can be adjusted individually to compensate for this – removing the need to run standards at multiple resolution settings on multiple instruments.

In Fig. 3, application of these fitting parameters gives a result of 25% Cu(0), 63% Cu_2O, and 13% $Cu(OH)_2$. These results align well with the Cu $2p_{3/2}$ [Cu(0) + Cu(I)]:Cu(II) results (section 3.4) and O 1s spectra (not shown). In a second example shown in Fig. 4, the curve-fitting results in an assessment of 22% Cu(0), 65% Cu_2O, and 13% Cu_2S. These results also align well with the Cu $2p_{3/2}$ spectrum (which only shows a single sharp main peak [no shake-up peaks detected]), the O 1s spectrum (which shows mostly lattice oxides species), the S 2p spectrum (which shows only sulfide species, and the survey spectrum – which gives values of the amounts of sulfur and oxygen consistent with the stoichiometry and amounts of species suggested by the Cu $L_3M_{4,5}M_{4,5}$ curve-fitting results presented.

Oxide film thickness measurements

Analysis of thin films of copper oxides/hydroxides on copper metal or alloy surfaces often requires an estimation of film thickness. This section provides the needed parameters and equations to do this

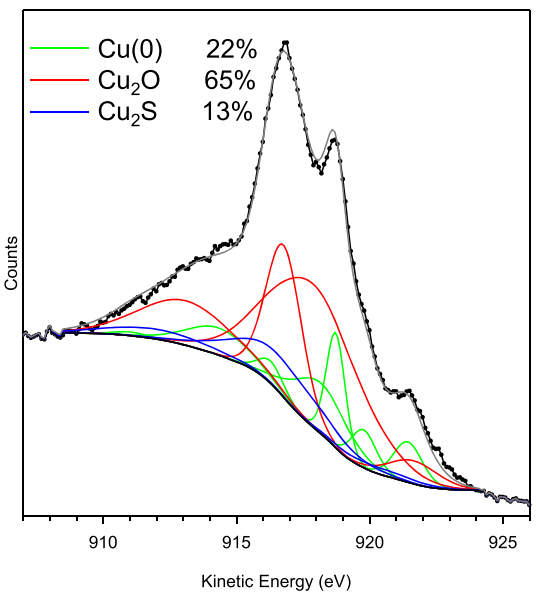

Figure 4. Curve-fitted Cu $L_3M_{4,5}M_{4,5}$ spectrum from a wrought copper sample submerged in an Ar aerated 3 M NaCl solution for 30 days. Curve-fitting results suggest 22% Cu(0), 65% Cu_2O, and 13% Cu_2S.

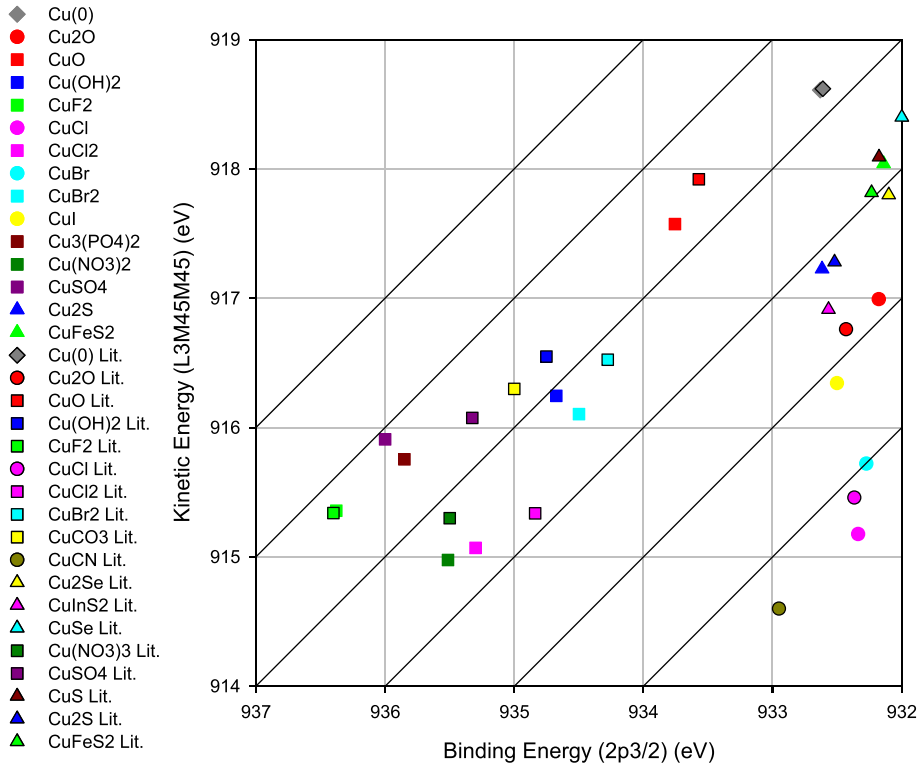

Figure 5. Cu $2p_{3/2}$ – Cu $L_3M_{4,5}M_{4,5}$ Wagner (chemical state) plot including literature (Table 1) and standard sample (Table 2) data.

using the results obtained from an analysis of the Cu LMM spectrum as completed in the section 3.5. IMFP values can be calculated using the NIST Electron Inelastic Mean Free Path Database (version 1.1) software[43] using the predictive formulae routines from Tanuma, Powell, and Penn.[44] For Cu_2O, CuO, and $Cu(OH)_2$ densities of 6.00, 6.31, and 3.37 g·cm^{-3} and band gap values of 2.1[45], 1.25 (ave. from[45,46]), and 1.85 eV[47] were used. For speciation results based on the Cu $L_3M_{4,5}M_{4,5}$ Auger line, a kinetic energy of 918 eV was used. These values result in IMFPs for Cu_2O, CuO, and $Cu(OH)_2$ of 1.77, 1.76, and 2.19 nm for Cu L_3 $M_{4,5}M_{4,5}$ Auger electrons, respectively. The IMFP for Cu(0) is 1.54 nm.

The appropriate IMFP values can then be applied for film thickness analysis for oxide depth (d) calculations of the type used by Carlson[48] and Strohmeier[49] defined as follows:

Table 6. Cu $2p_{3/2}$ binding energy, Cu $L_3M_{4,5}M_{4,5}$ kinetic energy, Auger parameter (α'), ΔE_b, ΔE_k, $\Delta\alpha'$, $\Delta\varepsilon$, and ΔR values

Compound	Cu $2p_{3/2}$ peak maximum E_b (eV)	Cu LMM Auger peak maximum E_k (eV)	Auger parameter (eV) (α')	ΔE_b (Cu $2p_{3/2}$)	ΔE_k (Cu LMM)	$\Delta\alpha'$	ΔR	$\Delta\varepsilon$
Cu(0)	932.63	918.61	1851.24	—	—	—	—	—
Cu_2O	932.18	916.99	1849.17	−0.45	−1.62	−2.07	−1.03	1.49
CuO	933.76	917.57	1851.33	1.13	−1.04	0.09	0.04	−1.17
$Cu(OH)_2$	934.67	916.25	1850.92	2.04	−2.36	−0.32	−0.16	−1.88
CuF_2	936.38	915.36	1851.74	3.75	−3.25	0.50	0.25	−4.00
CuCl	932.34	915.18	1847.51	−0.29	−3.43	−3.73	−1.86	2.16
$CuCl_2$	935.30	915.08	1850.37	2.66	−3.53	−0.87	−0.43	−2.23
CuBr	932.27	915.72	1848.00	−0.36	−2.89	−3.24	−1.62	1.98
$CuBr_2$	934.50	916.10	1850.60	1.87	−2.51	−0.64	−0.32	−1.55
CuI	932.50	916.34	1848.84	−0.13	−2.27	−2.40	−1.20	1.33
$Cu_3(PO_4)_2$	935.85	915.76	1851.61	3.22	−2.85	0.37	0.18	−3.40
$Cu(NO_3)_{2.3}H_2O$	935.51	914.98	1850.49	2.88	−3.63	−0.75	−0.38	−2.51
$CuSO_4$	936.00	915.91	1851.91	3.37	−2.70	0.67	0.34	−3.71
Chalcocite (Cu_2S)	932.62	917.23	1849.84	−0.01	−1.38	−1.40	−0.70	0.71
Chalcopyrite ($CuFeS_2$)	932.14	918.04	1850.18	−0.49	−0.57	−1.06	−0.53	1.02

$$d = \lambda_{ox} sin\phi \, ln(((N_m \lambda_m I_{ox})/(N_{ox} \lambda_{ox} I_m)) + 1) \quad (3)$$

where ϕ is the photoelectron take-off angle, I_{ox} and I_m are the area percentages of the oxide and metal peaks from the high-resolution spectrum, and N_m and N_{ox} are the volume densities of the metal atoms in the metal and oxide, respectively.

Considering an assumed uniformly mixed oxide/hydroxide thin film with known oxide, hydroxide, and metal concentrations (using the fitting procedures from the section 3.5) and given N_m/N_{Cu2O}, N_m/N_{CuO}, and $N_m/N_{Cu(OH)2}$ values of 1.68, 1.78, and 4.08 for Cu_2O, CuO, and $Cu(OH)_2$, respectively, Eqn (2) can be modified to include weighted averages of the three oxide/hydroxide IMFP (λ_{ave}) and volume density ratio components (N_{ave}) as follows:

$$d = \lambda_{ave} sin\phi \, ln\left(\left(\left(N_m \lambda_m \left(I_{Cu2O} + I_{CuO} + I_{Cu(OH)}\right)/\left(N_{ave} \lambda_{ave} I_m\right)\right) + 1\right)\right). \quad (4)$$

Using this calculation, the thin film from Fig. 3 with 63% Cu_2O, 13% $Cu(OH)_2$, and 25% metal would have a film thickness of ~3.2 nm. This is similar to work on oxide/hydroxide films on nickel samples employing Ni $2p_{3/2}$ curve-fitting routines.[11]

Cu $2p_{3/2}$ – Cu $L_3M_{4,5}M_{4,5}$ Wagner plot

The graphical display (scatter plot) of the most intense photoelectron line binding energies (abscissa, oriented in the negative direction) *versus* the kinetic energy position of the sharpest core–core–core Auger line (ordinate) is known as a Wagner plot, chemical state plot, or chemical state diagram. Positions of compounds on these plots indicate both relaxation energy and initial state effects.[50] Hence, the modified Auger parameter can be used in addition to the BE envelope to give additional insight into the shift in electronic state between metal compounds.

Cu $2p_{3/2}$ BE and Cu $L_3M_{4,5}M_{4,5}$ kinetic energy data from these samples (Table 2) and from literature average values (Table 1) were used to produce the Wagner (chemical state) plot presented in Fig. 5. As reported previously by Moretti,[51] two distinct trends can be seen. Compounds with a + 2 oxidation number generally follow the line with a slope of 1 and have similar Auger Parameter values. Compounds with a + 1 oxidation number are closer to the line with a slope of 3 and have similar BE values. These results would indicate that copper compounds with a + 2 oxidation number have similar final state effects but different initial state effects. Conversely, copper compounds with a + 1 oxidation number have similar initial state effects and different final state effects.[41,42,51] Further calculations involving the obtained BE, KE, and Auger parameter values can be carried out to obtain the relaxation shifts ($\Delta\alpha'$), initial state contributions ($\Delta\varepsilon$), and final state contributions (ΔR) of the various species (Table 6). Initial state effects, $\Delta\varepsilon$, are generally understood to represent the 'chemical shift' as a result of ground state electronic structure and are a function of the valence structure of the core atom, which in turn is a function of bonding to neighboring atomic valence states. These shifts are related to the electronic states (e.g. band structures and bond directionality) and structural parameters (e.g. atomic positions and Madelung constants) of the bonded atoms. Final state effects result from differences in polarization within the electron cloud of the atom after it has been ionized by X-ray irradiation. Final state effects are often dominant when dealing with compounds that have the potential for significant polarization or electron motility. See references [41,42,51] for calculation details and further in depth explanation.

Anions

Anion BE, FWHM, and Gaussian–Lorentzian peak-shape values obtained for the standard samples are presented in Table 3. For Cu_2O and CuO oxide samples, there is a second higher BE peak that can be ascribed to contributions from a defective oxide component inherent in these oxide surfaces as suggested previously.[7,8] Other work has shown that this is a defective oxide peak and not hydroxide as the presence of hydroxide has been ruled out by other methods.[52,53] For these oxides studied here, this peak has an area contribution between 32% and 36% consistent with other powdered oxides including nickel and chromium studied previously.[8,9,11] These contributions from defective sites are unlikely to compromise the assignment of chemical states. It should be noted that this second peak could result from carbonates species in unknown sample analyses.[5,6] Inspection of the C 1s spectrum should confirm if this is occurring or if other significant oxygen containing carbon species are present. In-depth analyses of the O 1s spectrum for copper and other transition metals are available in our previous work.[7–9,11,54,55]

Conclusions

Several strategies have been presented to overcome some of the complexities of assigning and quantifying copper species by XPS. Using a variety of approaches and incorporation of all available data has allowed for a more complete analysis of copper-based materials. Strategies have been presented that include as follows: an analysis of binding energies and Auger parameter values, practical advanced curve-fitting techniques applied to the Cu $2p_{3/2}$ and Cu $L_3M_{4,5}M_{4,5}$ spectra, and measurements of mix oxide/hydroxide surface film thickness. These procedures are based on a critical evaluation of existing literature and on high-resolution analyses of well-characterized standards.

Acknowledgements

This research was funded in part under the Industrial Research Chair agreement between the Natural Science and Engineering Research Council (NSERC, Ottawa) and the Nuclear Waste Management Organization (NWMO, Toronto).

References

[1] J. Doebrich, *Copper–A Metal for the Ages: U.S. Geological Survey Fact Sheet 2009-3031*, https://pubs.usgs.gov/fs/2009/3031/ **2009**.
[2] http://minerals.usgs.gov/minerals/pubs/commodity/copper/index.html
[3] P. G. Keech, P. Vo, S. Ramamurthy, J. Chen, R. Jacklin, D. W. Shoesmith, *Corros. Eng. Sci. Techn.*, **2014**, *49*, 425.
[4] M. d'Halluin, T. Mabit, N. Fairley, V. Fernandez, M. B. Gawande, E. Le Grognec, F.-X. Felpin, *Carbon*, **2015**, *93*, 974.
[5] C.D. Wagner, A.V. Naumkin, A. Kraut-Vass, J.W. Allison, C.J. Powell, J. R. Jr. Rumble, *NIST Standard Reference Database 20, Version 3.4 (web version)* (http:/srdata.nist.gov/xps/) **2003**.
[6] J. F. Moulder, W. F. Stickle, P. E. Sobol, K. D. Bomben, *Handbook of X-ray Photoelectron Spectroscopy*, Perkin-Elmer Corp, Eden Prairie, MN, **1992**.
[7] M. C. Biesinger, L. W. M. Lau, A. R. Gerson, R. S. C. Smart, *Appl. Surf. Sci.*, **2010**, *257*, 887.
[8] M. C. Biesinger, B. P. Payne, A. P. Grosvenor, L. W. M. Lau, A. R. Gerson, R. S. C. Smart, *Appl. Surf. Sci.*, **2011**, *257*, 2717.
[9] M. C. Biesinger, C. Brown, J. R. Mycroft, R. D. Davidson, N. S. McIntyre, *Surf. Interface Anal.*, **2004**, *36*, 1550.
[10] A. P. Grosvenor, B. A. Kobe, M. C. Biesinger, N. S. McIntyre, *Surf. Interface Anal.*, **2004**, *36*, 1564.

[11] M. C. Biesinger, B. P. Payne, L. W. M. Lau, A. Gerson, R. S. C. Smart, *Surf. Interface Anal.*, **2009**, *41*, 324.
[12] A. P. Grosvenor, M. C. Biesinger, R. S. C. Smart, N. S. McIntyre, *Surf. Sci.*, **2006**, *600*(9), 1771.
[13] C. J. Powell, A. Jablonski, *J. Electron Spectrosc. Relat. Phenom.*, **2010**, *178-179*, 331.
[14] S. Tougaard, *Surf. Interface Anal.*, **1998**, *26*, 249.
[15] A. Frydman, D. G. Castner, M. Schmal, C. T. Campbell, *J. Catal.*, **1995**, *157*, 133.
[16] B. P. Payne, A. P. Grosvenor, M. C. Biesinger, B. A. Kobe, N. S. McIntyre, *Surf. Interface Anal.*, **2007**, *39*, 582.
[17] A. P. Grosvenor, B. A. Kobe, N. S. McIntyre, *Surf. Interface Anal.*, **2004**, *36*, 1637.
[18] A. P. Grosvenor, J. T. Francis, B. A. Kobe, N. S. McIntyre, *Surf. Interface Anal.*, **2005**, *37*, 495.
[19] A. P. Grosvenor, B. A. Kobe, N. S. McIntyre, *Surf. Sci.*, **2005**, *574*, 317.
[20] D. J. Miller, M. C. Biesinger, N. S. McIntyre, *Surf. Interface Anal.*, **2002**, *33*, 299.
[21] N. Fairley, http://www.casaxps.com, © Casa software Ltd. (**2005**).
[22] D. Briggs, J. C. Rivière, in *Practical Surface Analysis by Auger and X-ray Photoelectron Spectroscopy* (Eds: D. Briggs, M. P. Seah), John Wiley & Sons, Chichester, UK, **1983**, p. 135.
[23] P. A. W. Van der Heide, *J. Electron Spectrosc. Relat. Phenom.*, **2008**, *164*, 8.
[24] S. W. Goh, A. N. Buckley, R. N. Lamb, R. A. Rosenberg, D. Moran, *Geochim. Cosmochim. Acta*, **2006**, *70*, 2210.
[25] S. Poulston, P. M. Parlett, P. Stone, M. Bowker, *Surf. Interface Anal.*, **1996**, *24*, 811.
[26] G. Lassaletta, A. Fernández, J. P. Espinós, A. R. González-Elipe, *J. Phys. Chem.*, **1995**, *99*, 1484.
[27] J. P. Espinós, J. Morales, A. Barranco, A. Caballero, J. P. Holgado, A. R. González-Elipe, *J. Phys. Chem. B*, **2002**, *106*, 6921.
[28] J. C. Otamiri, S. L. T. Andersson, A. Andersson, *Appl. Catal.*, **1990**, *65*, 159.
[29] P. Velásquez, D. Leinen, J. Pascual, J. R. Ramos-Barrado, P. Grez, H. Gómez, R. Schrebler, R. Del Río, R. J. Córdova, *Phys. Chem. B*, **2005**, *109*, 4977.
[30] S. Poulston, P. M. Parlett, P. Stone, M. Bowker, *Surf. Interface Anal.*, **1996**, *24*, 811.
[31] D. N. Wang, A. C. Miller, M. R. Notis, *Surf. Interface Anal.*, **1996**, *24*, 127.
[32] L. Meda, G. F. Cerofolini, *Surf. Interface Anal.*, **2004**, *36*, 756.
[33] L. Feng, L. Zhang, D. G. Evans, X. Duan, *Colliods Surf. A*, **2004**, *244*, 169.
[34] L. J. Kundakovic, M. Flytzani-Stephanopoulos, *Appl. Catal., A*, **1998**, *171*, 13.
[35] P. Salvador, J. L. G. Fierrom, J. Amador, C. Cascales, I. Rasines, *J. Solid State Chem.*, **1989**, *81*, 240.
[36] M. C. Biesinger, B. R. Hart, R. Polack, B. A. Kobe, R. S. C. Smart, *Miner. Eng.*, **2007**, *20*, 152.
[37] A. R. Gerson, M. Jasieniak, in *Proceedings of the XXIV International Minerals Processing Congress* (Eds: W. D. Duo, S. C. Yao, W. F. Liang, Z. L. Cheng, H. Long), Science Press, Beijing, Beijing, China, **2008**, pp. 1054–1063.
[38] J. F. Watts, J. Wolstenholme, *An Introduction to Surface Analysis by XPS and AES*, Wiley, Rexdale, **2003**, p. 71.
[39] G. Deroubaix, P. Marcus, *Surf. Interface Anal.*, **1992**, *18*, 39.
[40] S. Saikova, S. Vorobyev, M. Likhatski, A. Romanchenko, S. Erenburg, S. Trubina, Y. Mikhlin, *Appl. Surf. Sci.*, **2012**, *258*, 8214.
[41] M. C. Biesinger, L. W. M. Lau, A. R. Gerson, R. S. C. Smart, *Phys. Chem. Chem. Phys.*, **2012**, *14*(7), 2434.
[42] J. L. Bourque, M. C. Biesinger, K. M. Baines, *Dalton Trans.*, **2016**, *45*, 7678.
[43] *NIST Electron Inelastic Mean Free Path Database (Version 1.1)* © U.S. secretary of commerce **2000**.
[44] S. Tanuma, C. J. Powell, D. R. Penn, *Surf. Interface Anal.*, **1991**, *17*, 927.
[45] M. A. Rafea, N. Roushdy, J. Phys, *D: Appl. Phys.*, **2009**, *42*, 015413.
[46] L. Wang, K. Han, G. Song, X. Yang, M. Tao, IEEE, 130-133, **2006**
[47] F. Di Quarto, M. C. Romano, M. Santamaria, S. Piazza, C. Sunseri, *Russ. J. Electrochem.*, **2000**, *36*, 1203.
[48] T. A. Carlson, G. E. McGuire, J. Electron, *Spectrosc. Relat. Phenom.*, **1972**/73, *1*, 161.
[49] B. R. Strohmeier, *Surf. Interface Anal.*, **1990**, *15*, 51.
[50] G. Moretti, *J. Electron Spectrosc. Relat. Phenon.*, **1998**, *95*, 95.
[51] G. Moretti, *Surf. Sci.*, **2013**, *618*, 3.
[52] H. A. E. Hagelin-Weaver, J. F. Weaver, G. B. Hoflund, G. N. Salaita, *J. Electron Spectrosc. Relat. Phenon.*, **2004**, *134*, 139.
[53] P. R. Norton, G. L. Tapping, J. W. Goodale, *Surf. Sci.*, **1977**, *65*, 13.
[54] B. P. Payne, M. C. Biesinger, N. S. McIntrye, *J. Electron Spectrosc. Relat. Phenon.*, **2011**, *184*, 29.
[55] B. P. Payne, M. C. Biesinger, N. S. McIntrye, *J. Electron Spectrosc. Relat. Phenon.*, **2012**, *185*, 159.

Appendix I: Selected XPS survey scan results in atomic percent

	C	N	O	F	Na	P	S	Cl	Ca	Fe	Cu	Zn	Br	Ag	Sn	I	Pb
Cu_2O	65.7	—	21.2	—	—	—	—	—	—	—	11.9	0.8	—	—	—	—	0.4
CuO	20.3	—	42.5	—	—	—	—	—	—	—	37.1	—	—	—	—	—	—
$Cu(OH)_2$	23.0	—	49.4	—	—	—	—	2.8	—	—	24.8	—	—	—	—	—	—
CuF_2	16.6	—	8.7	45.1	—	—	—	—	—	—	29.6	—	—	—	—	—	—
CuCl	25.8	—	2.8	—	—	—	—	34.3	—	—	37.1	—	—	—	—	—	—
$CuCl_2$	8.5	—	5.0	—	—	—	—	56.8	—	—	29.7	—	—	—	—	—	—
CuBr	25.6	—	5.2	—	—	—	—	—	—	—	34.1	—	35.1	—	—	—	—
$CuBr_2$	39.5	—	12.4	—	—	—	—	—	—	—	16.9	—	30.9	—	0.2	—	—
CuI	37.4	—	2.0	—	—	—	—	—	—	—	23.8	—	—	—	—	36.9	—
$Cu_3(PO_4)_2$	15.3	—	53.5	—	0.3	11.9	—	—	—	—	19.0	—	—	—	—	—	—
$Cu(NO_3)_{2.3}H_2O$	11.9	18.0	52.9	—	—	—	—	—	—	—	17.2	—	—	—	—	—	—
$CuSO_4$	16.8	—	57.2	—	—	—	12.8	—	—	—	13.1	—	—	—	—	—	—
Chalcocite (Cu_2S)	24.3	—	22.7[a]	—	—	—	16.1	—	—	—	33.6	—	—	3.2	—	—	—
Chalcopyrite ($CuFeS_2$)	25.8	—	4.6	—	2.1	—	27.7	9.5	3.0	13.2	13.9	—	—	—	—	—	—

[a]Mostly present as carbonate.